Journal of Applied Physics

RESEARCH ARTICLE | MARCH 15 2023

Thermal rectification in thin film metalattice structures: A computational study

Devon A. Eichfeld ✉; Weinan Chen; Ismaila Dabo; ... et. al

Journal of Applied Physics 133, 115101 (2023)
https://doi.org/10.1063/5.0135963

AIP Publishing

Journal of Applied Physics ARTICLE scitation.org/journal/jap

Thermal rectification in thin film metalattice structures: A computational study

Cite as: J. Appl. Phys. **133**, 115101 (2023); doi: 10.1063/5.0135963
Submitted: 23 November 2022 · Accepted: 23 February 2023 ·
Published Online: 15 March 2023

Devon A. Eichfeld,[1,2,a)] Weinan Chen,[2,3,4] Ismaila Dabo,[2,3] Brian M. Foley,[5] and Bladimir Ramos-Alvarado[1,a)]

AFFILIATIONS

[1]Department of Mechanical Engineering, The Pennsylvania State University, University Park, Pennsylvania 16802, USA
[2]Materials Research Institute, The Pennsylvania State University, University Park, Pennsylvania 16802, USA
[3]Department of Materials Science and Engineering, The Pennsylvania State University, University Park, Pennsylvania 16802, USA
[4]Institute of Computational and Data Sciences, The Pennsylvania State University, University Park, Pennsylvania 16802, USA
[5]Laser Thermal, Charlottesville, Virginia 22902, USA

[a)]**Authors to whom correspondence should be addressed:** dae96@psu.edu and bzr52@psu.edu

ABSTRACT

Thermal rectification is an asymmetric heat transfer process where directionally dependent transport occurs along a given axis. In this work, geometric parameters that govern thermal rectification in solids composed of various semiconducting materials were investigated utilizing metalattice data for seven materials with pore sizes ranging between 2 and 30 nm. Using numerical simulation, thermal rectification was calculated at different thermal biases in single material systems, including silicon, cubic boron nitride, and diamond, among others. The largest thermal rectification for each material was exhibited in bilayer sample stacks that were thermally matched (i.e., the thermal resistance of each layer in the stack is equal in either forward or reverse direction). Of the materials tested, diamond provided the highest thermal rectification for all cases, with its best case achieving a thermal rectification of 57.2%. This novel thermal functionality will find application in advanced applications for temperature regulation, including resonator systems where thermal effects may significantly alter and/or degrade performance.

I. INTRODUCTION

Thermal rectification is a phenomenon where the heat flow on an axis varies based on the direction of the temperature gradient. With growing interest in developing thermally driven phononics[1,2] (analogous to electronics), thermal rectifiers have received notable interest; however, various parameters in rectifier design have yet to be thoroughly investigated. Thermal rectifiers have been modelled[3–14] and demonstrated experimentally,[14–17] with rectification values up to ~350% at the nanoscale,[8] but only modest thermal rectification has been achieved at larger length scales thus far. Among solid thermal rectifiers, Dames[4] described the concept of thermal matching between two segments of different materials to achieve maximum thermal rectification by matching the thermal resistance in either segment based on the heat flow in both directions and by selecting materials with opposite power-law behavior for their temperature-dependent thermal conductivities. Sawaki *et al.*[14] explored the geometric dependence of thermal rectification in bi-material systems, noting that a rectangular-shaped sample outperformed a pyramidal-shaped sample of same materials in experiments, and Li and Ren[11] predicted a high-performance thermal rectifier at the nanoscale using asymmetric "diode" geometries to limit reverse wave propagation between two nonlinear materials. Within single material systems, several studies[5–7,17] have demonstrated thermal rectification through careful structuring of the material in both, macro- and nano-scales. Among these, Cheng *et al.*[5] showed that polycrystalline diamond grown through chemical vapor deposition (CVD) exhibits natural thermal rectification due to variation in thermal conductivity (κ) due to the graded grain size; thus, heat flows preferentially from the nucleation side to the growth side of the crystal, exhibiting thermal rectification up to 25% with a 200 K thermal bias centered at 275 K. This model provides a basis to explore a single-material system where the mean-free paths (MFPs) of phonons are arrested strategically to induce thermal rectification.

Recent work in generating and studying the material properties of pore size-controlled metalattices has provided a simple pathway to engineer microstructures with tailored material properties.[18,19] Metalattices are crystalline structures that are composed of periodically placed pores of a given size. By controlling the pore size of the material, the MFPs of phonons in the structure are limited, enabling the thermal conductivity of a single material (e.g., boron arsenide) to be tuned within a range that spans up to three orders of magnitude between bulk and pore size with the minimum thermal conductivity.[19] Furthermore, metalattice pore sizes can be graded in a single structure during synthesis, creating an opportunity to design a structure with variable thermal conductivity between different regions. Metalattices also demonstrate an absolute minimum in thermal conductivity at a pore size of ~10 nm due to Mie scattering of phonons.[19] Metalattices with much smaller pores (e.g., 2 nm) exhibit significantly higher thermal conductivities at the same temperature than in ~10 nm pore size structures. This behavior is attributed to Rayleigh scattering, where the size of the defects decreases and the material looks more bulk-like from a thermal standpoint.[19] The unique ability to tune the thermal conductivity in metalattice structures may enable the design of high performance, thin-film thermal rectifiers.

In this work, we investigated a new design space for solid thermal rectifiers by utilizing the tunable properties of novel metalattice structures. By leveraging thermal conductivity data from first-principles based ballistic modeling for metalattice pore sizes ranging between 2 and 30 nm using various semiconducting materials of high interest as the host material, including silicon, cubic boron nitride, and diamond, we performed numerical simulations to calculate thermal rectification in 1-D geometry sample structures. These test case structures were chosen to help illustrate how to optimize thermal rectification using novel metalattices, including simple bilayers and complicated multilayer structures. Examining each test case at four different thermal biases around 275 K, we predict that high performing, thin-film thermal rectifiers can be generated using well-optimized metalattice structures. Our data indicated that bilayer structures can easily be tuned to optimize thermal rectification through matching the thermal resistance of each layer. Notably, silicon metalattices exhibited performance up to 19% rectification using a thermally matched bilayer structure of 2 nm pore metalattice and bulk layers, which would be relatively easy to physically realize, while cubic boron nitride and diamond achieved over 50% rectification using a bilayer of 2 and 30 nm pore sizes. These results have implications toward further optimization of thermal rectifiers through tuning thermal material properties and device design.

II. METHODS

A. Finite element model

Thermal rectification was calculated by Fourier's law, following a similar procedure to those employed by Peyrard *et al.*[3] and Cheng *et al.*[5] A finite element method was used to calculate steady state 1-D heat conduction through a metalattice sample. Each sample was discretized into N mesh layers of constant thickness, dz. Using an initial guess for the heat flux through the sample (q_o), the temperature for each mesh layer was calculated consecutively by

$$T_{i+1} = T_i - \frac{q_0}{\kappa_i} dz, \tag{1}$$

where T_i and T_{i+1} are the respective temperatures at top and bottom bounds of layer i, κ_i is the thermal conductivity of the mesh layer i, and dz is the mesh layer thickness. The thermal conductivity of each layer was determined based on the layer's pore size and its top surface temperature. Using only the top surface temperature to calculate κ_i does not introduce significant error because the change in temperature in a given layer is small (<1 K), as each sample was equally divided into 10 000 mesh layers with a maximum thermal bias of 200 K across the sample. Once the temperature of each layer has been computed, a new iteration for q_0 is performed based on the desired temperature drop (thermal bias) across the sample stack relative to the overall thermal resistance of the sample stack, and the process is repeated until the solution converges.

Within this model, sample layers that possess different properties (i.e., grain size or metalattice pore size) are assumed to be in perfect contact, thus producing negligible thermal contact resistance between sample layers. This approximation may be a source of error; however, each case in the present work consists of a single-material system that minimizes the acoustic and diffuse phononic mismatch between sample layers (driving forces behind contact resistance).[4,20] Similar assumptions (e.g., "perfect contacts") are made in other studies.[3,4,14]

The results of this work are presented as thermal rectification, as demonstrated in Fig. 1(a), which is defined as

$$\mathcal{R}_{TR} = \frac{R_i - R_j}{R_j}, \tag{2}$$

where R_i is the thermal resistance in the sample of the heat flow in either the forward left-to-right or reverse right-to-left direction, whichever is greater, and R_j is the thermal resistance of the heat flow in the opposite direction. Figure 1(b) depicts a bilayer test case investigated in this work that is further described in Sec. II C.

B. Validation

The finite element method described in Sec. II A was validated against thermal rectification calculations of CVD diamond obtained from Cheng *et al.*[5] Thermal conductivity data for CVD diamond were generated using the phonon-gas model with full-phonon dispersion curves.[21,22] Specific heat C_v and thermal conductivity κ were calculated from the dispersion data by

$$C_v = \frac{1}{2\pi^2} \sum_j \int_k \hbar\omega_j \frac{\partial f_{BE}}{\partial T} k^2 dk, \tag{3}$$

$$\kappa = \frac{1}{6\pi^2} \sum_j \int_k \hbar\omega_j \frac{\partial f_{BE}}{\partial T} v_j^2 \tau_j k^2 dk, \tag{4}$$

where j indicates phonon polarization, ω is the angular frequency, k

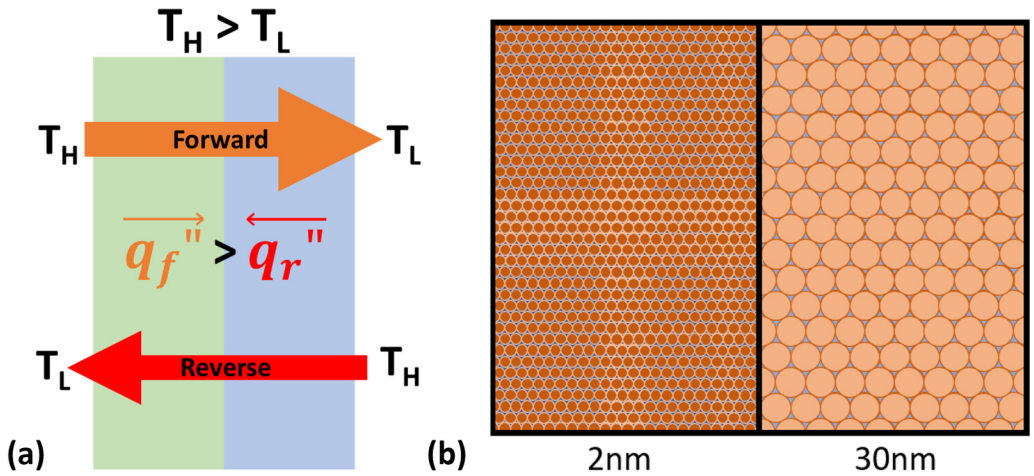

FIG. 1. (a) Schematic demonstrating how thermal rectification occurs within a material where, q_f" and q_r" represent forward and reverse heat fluxes, respectively, and (b) proposed geometry for test case 3, showing a 1:1 layer ratio between 2 and 30 nm pore size metalattices.

is the phonon wavevector, v is the phonon group velocity, $\hbar$ is the reduced Planck's constant, f_{BE} is the Bose–Einstein distribution, and τ is the total scattering rate, given by Matthiessen's rule,[23]

$$\tau_j = \left[\frac{1}{\tau_{imp}} + \frac{1}{\tau_u} + \frac{v_j}{d}\right]^{-1}, \tag{5}$$

where d is the average grain size; τ_{imp} is the impurity scattering term given by $\tau_{imp} = (A\omega_j^4)^{-1}$; τ_u is the Umklapp scattering term given by $\tau_u = (BT\omega_j^2 \exp(-C/T))^{-1}$; and A, B, and C are fitting parameters for scattering rates, which were chosen as 1.15×10^{-46} s^3, 2.2×10^{-20} s K^{-1}, and 610 K, respectively, to best match the data presented in Cheng *et al.*[5] It should be noted that the Umklapp scattering term, τ_u, is primarily what drives the non-linear temperature-dependence of thermal conductivity due to its suppression of high energy, large wavevector phonons at high temperatures as the phonon density of states fill.[23] As shown in Fig. 2(a), a perfect fit was not acquired due to differences in phonon-gas model assumptions (different phonon dispersion data may have been used, Cheng *et al.* considered anisotropic cross-plane thermal conductivity while this model assumes isotropy). The quality of the fit is overall good in the temperature range of interest, roughly 150–400 K; however, there are some discrepancies near the edges of this range, and the mid-size grains (e.g., 5 and 15 μm) are slightly off in magnitude.

Using the calculated thermal conductivity data for CVD diamond, thermal rectification was computed for same cases as those presented by Cheng *et al.*[5] The calculated thermal rectification values are in good agreement, with each test case demonstrating the same trends with similar magnitude, see Fig. 2(b). Differences in the data are greater at smaller grain sizes [e.g., shallow depth into the seeded crystal seen in Fig. 2(b)], and the 175–375 K test case varies the most between the reported and

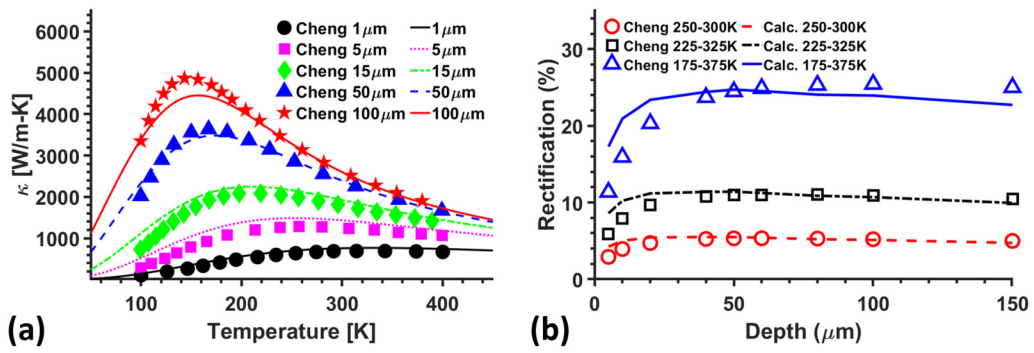

FIG. 2. (a) Fitted phonon-gas model thermal conductivity data (lines) for different grain sizes and (b) numerically calculated thermal rectification (lines) as compared to results from Cheng *et al.*[4] (symbols).

calculated thermal rectification. These discrepancies are expected to be a result from the imperfect fit for the thermal conductivity data in the phonon-gas model.

Finally, the finite element method used in this work was self-consistent, yielding thermal rectification percentages within ~0.5% between test cases of N layers, where N is equal to 1000, 10 000, and 100 000 mesh layers or where dz is chosen to be 1 or 0.1 nm. These data are provided in Table S1 in the supplementary material. Based on this data, a mesh of 10 000 layers was used for each test case to ensure reliable convergence.

C. Test cases

Table I summarizes test parameters employed to determine the thermal rectification behavior in simple-geometry (1-D) structures composed of metalattices of different pore size combinations among seven different semiconducting materials including silicon (Si), germanium (Ge), gallium arsenide (GaAs), boron arsenide (BAs), cubic boron nitride (cBN), germanium carbide (GeC), and diamond. Through first-principles-based ballistic modeling described by Chen *et al.*,[19] temperature-dependent thermal conductivity data were generated for the bulk material and metalattice pore sizes of radii 2 through 30 nm in 2 nm increments for each of these materials. See the supplementary material for details on the ballistic theory modeling efforts and calculations. The temperature-dependent thermal conductivity for select pore sizes and bulk for each material are depicted in Figs. S3 and S4 in the supplementary material.

Each test case examines only a single-material system. The first two cases explore the effect of combining each available pore size to understand trends of temperature and thermal conductivity through a complex, graded stack. These cases are as follows: (1) a 1.5 μm sample stack consisting of a 100 nm layer for each pore size in ascending order, and (2) a 0.48 μm sample stack consisting of a layer for each pore size that has a thickness equivalent to the diameter of each given pore size (i.e., the 10 nm pore size has a layer thickness of 20 nm). The other four cases explore bilayer/heterojunction combinations of different pore sizes, with a total sample stack thickness of 10 μm but varying layer thicknesses. These cases include the following: (3) 5 μm layers of each 2 and 30 nm pore sizes, (4) thermally matched layers of 2 and 30 nm pore size layers (i.e., the thermal resistance of each layer is equal),[4] (5) thermally matched 2 nm pore size and "bulk" layers, and (6) thermally matched layers of the 2 nm pore size and the minimum thermal conductivity pore size (e.g., the 10 nm pore size) for that material. Each test case was evaluated at four thermal biases (50, 100, 150, and 200 K), each centered around 275 K. For each thermally matched bilayer test case, thermal matching was determined numerically by changing the relative thickness of each sample layer until the bilayer interface temperature was equal to the central temperature of 275 K, thus ensuring equal thermal resistance in each layer.

III. RESULTS

Figures 3(a) and 3(b) depict examples of some key results from this study. Figure 3(a) demonstrates the results of six test cases for Si. Si achieves low thermal rectification in cases 1 and 2 (approximately 3% and 1.5%, respectively, with a 200 K bias). In case 3, Si achieves some improvement over cases 1 and 2, with approximately 6.7% rectification at 200 K bias. Finally, in cases 4, 5, and 6, Si demonstrates a much higher rectification of 15.2%, 19.3%, and 14.2%, respectively, at a 200 K bias. There is a twofold increase in thermal rectification between cases 3 and 4, where the only variable that changed was the layer thickness. In all test cases, Si shows a relatively linear increase in rectification with increasing thermal bias, with maximum rectification at the maximum 200 K bias.

Figure 3(b) demonstrates the performance of all materials in a single test case, case 4 with thermally matched layers. This cross-material comparison helps illustrate how the unique properties of each material affect their performance as metalattice-based thermal rectifiers. Here, it can be seen that Si and the

TABLE I. Test matrix including the parameters and test cases considered in this work.

Test parameters			
Materials			Metalattice pore sizes (PS)
Silicon (Si)	Germanium carbide (GeC)		2, 4, 6, …, 28, 30 nm; bulk
Germanium (Ge)	Cubic boron nitride (cBN)		
Gallium arsenide (GaAs)	Diamond		Thermal biases (centered at $T_c = 275$ K)
Boron arsenide (BAs)			50, 100, 150, and 200 K
Test cases (single material with multiple PS calculated for all thermal biases)			
Case	Sample thickness (μm)	Sample layer thickness	Layer composition
1	1.5	0.1 μm	Graded PS (2, 4, …, 30 nm)
2	0.48	2× layer PS	Graded PS (2, 4, …, 30 nm)
3	10	5 μm	Bilayer: 2 nm, 30 nm
4	10	Thermally matched	Bilayer: 2 nm, 30 nm
5	10	Thermally matched	Bilayer: 2 nm, bulk
6	10	Thermally matched	Bilayer: 2 nm, minimum κ pore size (e.g., 10 nm)

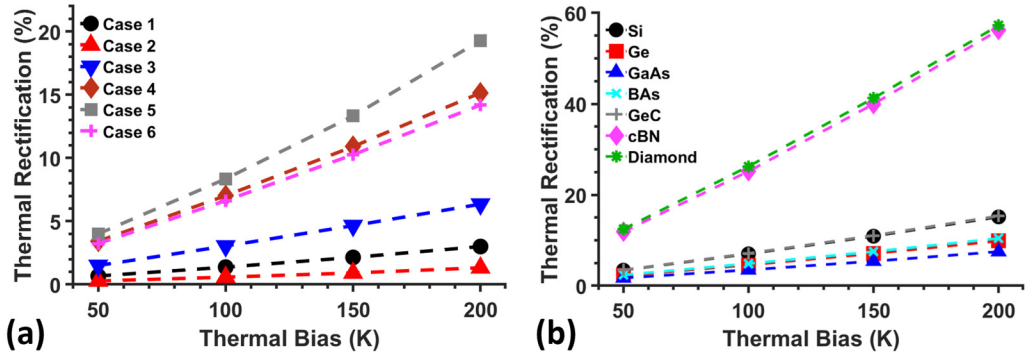

FIG. 3. (a) Thermal rectification data for Si metalattices in all cases and (b) all tested materials for test case 4.

other materials tested behaved similarly, with the exception of cBN and diamond. It is demonstrated that thermal rectification increases approximately linearly with increasing thermal bias for each material. It is also apparent that Si, Ge, GaAs, BAs, and GeC perform similarly (achieving approximately 14.2%, 9.6%, 7.5%, 8.4%, and 13.6%, respectively, at 200 K bias), while cBN and diamond demonstrate much higher rectification than the other materials in most cases. These trends are noted throughout this work.

The calculated thermal recitification for all test cases is reported in Table II. Comparing Si with other materials tested, Ge, GaAs, BAs, and GeC each demonstrates similar rectification performance in all cases. For each case, the thermal rectification for Ge, GaAs, BAs, and GeC falls within approximately 50% of the rectification that Si achieves for the same test case, except for BAs in cases 1 and 5 (4.78% and 4.92% rectification, respectively, compared to Si with 3.00% and 19.29%, respectively) and Ge in case 2 (0.34% rectification compared to Si with 1.32%).

TABLE II. Thermal rectification data for each test. Cells are shaded according to the degree of thermal rectification: no highlight (<10%), light green (10%–20%), green (20%–30%), and dark green (>30%). Text is bold for cases above 50% rectification.

Case number	Thermal bias (K)	Temperature range (K)	Si (%)	Ge (%)	GaAs (%)	Bas (%)	GeC (%)	cBN (%)	Diamond (%)
Case 1	150	250–300	0.67	0.37	0.57	1.12	0.84	3.38	3.90
	100	225–325	1.37	0.76	1.16	2.27	1.72	6.87	7.91
	150	200–350	2.14	1.18	1.79	3.48	2.64	10.43	11.95
	200	175–375	3.00	1.67	2.49	4.78	3.64	14.02	15.95
Case 2	50	250–300	0.28	0.06	0.16	0.56	0.41	1.98	2.42
	100	225–325	0.58	0.13	0.33	1.13	0.83	4.01	4.87
	150	200–350	0.91	0.22	0.52	1.74	1.28	6.10	7.35
	200	175–375	1.32	0.34	0.74	2.39	1.79	8.22	9.79
Case 3	50	250–300	1.50	1.49	1.18	1.32	1.52	3.14	2.42
	100	225–325	3.04	3.05	2.40	2.69	3.08	6.28	4.84
	150	200–350	4.65	4.69	3.71	4.14	4.71	9.34	7.22
	200	175–375	6.35	6.49	5.14	5.72	6.43	12.24	9.51
Case 4	50	250–300	3.42	2.24	1.71	2.38	3.47	11.86	12.45
	100	225–325	7.02	4.58	3.49	4.86	7.12	25.15	26.24
	150	200–350	10.90	7.09	5.40	7.51	11.05	39.96	41.25
	200	175–375	15.15	9.86	7.50	10.42	15.35	**56.21**	**57.23**
Case 5	50	250–300	4.00	3.16	3.55	1.22	2.23	2.83	4.07
	100	225–325	8.35	6.51	7.32	2.44	4.51	5.75	8.95
	150	200–350	13.32	10.15	11.42	3.67	6.88	9.90	15.48
	200	175–375	19.29	14.24	16.02	4.92	9.33	16.52	24.72
Case 6	50	250–300	3.23	2.21	1.72	1.92	3.11	9.36	9.20
	100	225–325	6.63	4.52	3.50	3.92	6.36	19.61	19.08
	150	200–350	10.26	6.97	5.40	6.05	9.83	30.76	29.46
	200	175–375	14.19	9.63	7.46	8.38	13.61	42.67	40.16

With the exception of cases 3 and 5, cBN and diamond significantly exceed the performance of any other tested materials (approximately 3–6 times higher rectification than Si), with maximum rectification of 56.2% and 57.2% in case 4 at a 200 K bias, respectively. These trends deviate in case 3, cBN and diamond demonstrate 100% and 50% more rectification than Si, respectively, and in case 5, cBN and diamond achieved 20% less and 40% more rectification than Si, respectively.

IV. DISCUSSION

The data for Si under cases 1 and 2 show that having multiple layers in the sample stack inhibit overall thermal rectification as compared to relatively simple bilayer cases. Additionally, it was found that by thermally matching the bilayers or adjusting the layer thickness of each layer such that each layer has the same resistance, these bilayers can achieve significantly higher rectification. This behavior was observed between cases 3 and 4 for Si and GeC data, where rectification of similar bilayer systems more than doubles when layer thicknesses are adjusted to be thermally matched. When the ratio in case 3 is closer to thermally matched, there is a smaller increase in rectification between moving from case 3 to case 4, as shown in data for Ge and GaAs. These findings are in support of conclusions drawn by Dames[4] regarding thermal matching and optimal rectification.

To further understand the mechanism of thermal matching, both temperature and thermal conductivity profiles within the sample for cases 3 and 4 are shown in Figs. 4(a) and 4(b). In case 3 where the layers are of equal thickness, the temperature at the interface varies based on the direction of the heat flow. Furthermore, because the thermal conductivity is a function of temperature, the thermal conductivity near the interface in either layer also varies substantially based on the direction of the heat flow. These observations are accompanied by a thermal rectification of 7%. However, when the thermal resistances of each layer are matched (by designing a specific layer thickness ratio) such as in case 4, the temperatures and thermal conductivities at the interface converge for both forward and reverse heat flows. In the case of Si, the thermal rectification reaches a maximum at ~15% rectification, doubling the performance from case 3. Figure 4(c) shows how thermal rectification varies with layer thickness ratio for each thermal bias around 275 K; for each bias, there is a peak that shifts slightly based on the temperature-dependence of the thermal conductivity for Si. For the 200 K bias case in Si, the peak in thermal rectification is found at a ratio of 88:12 for the 2-30 nm layers. For the 200 K bias in case 4, thermal matching was achieved by using following layer thickness ratios for 2–30 nm layers for each other material: Ge (79:21), GaAs (78:22), BAs (84:16), cBN (93:7), GeC (88:12), and diamond (95:5).

It is expected that extending the geometry of the sample beyond a simple, effective 1-D stack and focusing on thermally matching the layers in the system will enable tuned and higher performing thermal rectifiers. Additional work should be performed in optimizing multi-layer systems of three or more layers, including pore size selection, pore size layer ordering, and thermally matching these layers. Specifically since metalattices with intermediate pore sizes (e.g., 8–12 nm) demonstrate lower thermal conductivities than the extremes (2 and 30 nm), the ordering of layer thickness is expected to impact optimal thermal rectification conditions (layer thickness, thermal bias, center bias temperature, etc.).

Of the materials and cases investigated here, the highest rectification was achieved by cBN and diamond with rectification values up to

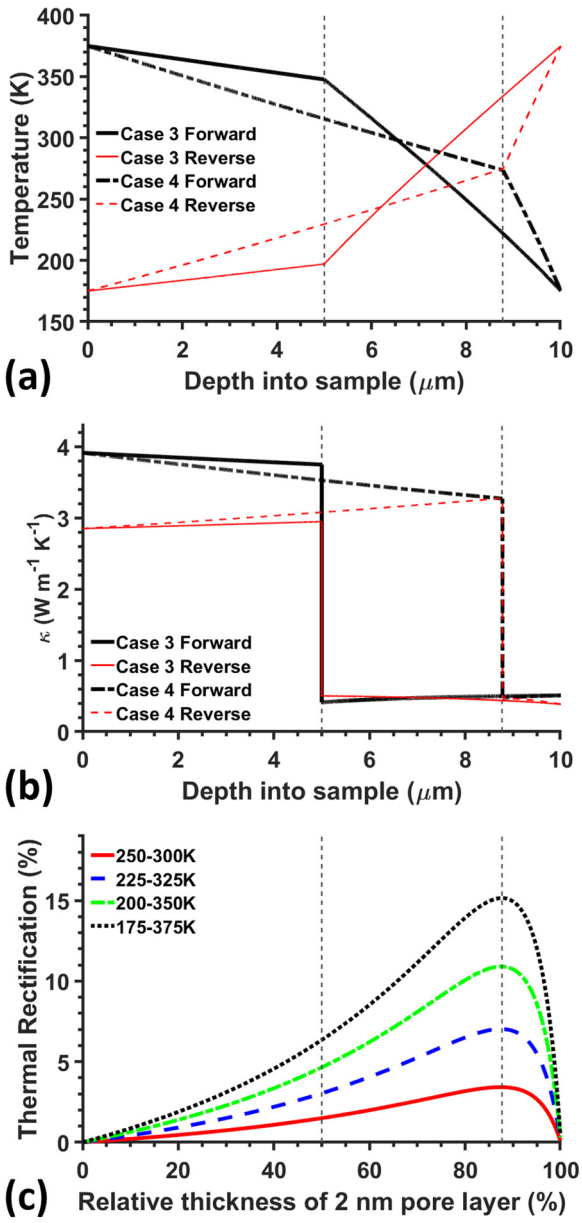

FIG. 4. Comparison between (a) temperature profiles and (b) thermal conductivity profiles within the samples of the 50:50 case 3 (solid lines) and thermally matched case 4 (dashed lines) in silicon metalattices, and (c) the thermal rectification over a thickness sweep of the ratio between 2 and 30 nm pore sizes. Vertical lines are given to indicate the interface location for case 3 (left) and case 4 (right).

56.21% and 57.23%, respectively. In each case, cBN and diamond tend to have rectification values that range between 3 and 4 times those of other materials for a given case, except for case 5, the bilayer system with a 2 nm pore size layer and a "bulk" layer. In case 5, cBN demonstrated approximately 20% lower rectification than Si and GeC, and diamond performs only about 40% higher than Si or GeC. The high performance of cBN and diamond metalattice rectifiers is likely related to the high Debye temperatures of cBN[24] and diamond,[25] over 1800 and 2200 K, respectively, compared to other materials that range between ~300 and 830 K.[23–26] Materials with high Debye temperatures tend to exhibit broader spectra of phonon modes, which cause these materials to require higher temperatures to saturate their phonon spectra. Thus, at same temperatures, these materials experience lower levels of scattering events (i.e., Umklapp scattering)[23] that give rise to anharmonic suppression of thermal conductivity in solids with rising temperature. This temperature-dependent behavior also extends to metalattices of cBN and diamond, where it is evident that phonon spectra that contribute to the total thermal conductivity of 2 and 30 nm pore size metalattices vary substantially when compared with materials such as Si (see Fig. S5 in the supplementary material). This variation also creates a larger difference in nonlinearities between different pore sizes of the same material and, thus, a greater opportunity to engineer the asymmetric heat flow as there should be greater mismatch between phonon populations between the two metalattice layers, similar to engineering nonlinear asymmetry through heterojunctions of dissimilar materials or by tailoring the geometry of the structure.[2,4,11]

There appears to be a strong correlation with Debye temperature and the peak temperature, width, and magnitude of the peak of maximum thermal conductivity for 2 nm pore size, as seen in Fig. 5(a). As illustrated, the materials with higher Debye temperatures tend to have thermal conductivity peaks that are both wider and occur at higher temperatures (e.g., ~300 K). Our data also indicate that when the peak in thermal conductivity is closer to and overlaps with the temperature range tested, the thermal rectifier will be more efficient. Looking at the 30 nm pore size data in Fig. 5(b), the thermal conductivity of materials with higher Debye temperatures appears to saturate at higher temperatures, further implying a stronger nonlinear temperature-dependence (and potential for thermal rectification) at near ambient temperatures as compared to other materials.

Dames[4] further explains how matching the power law exponents ($\kappa \propto T^n$) for bulk material bilayers impacts the overall thermal rectification of a simple, thermally matched 1-D system. Maximum thermal rectification is achieved when the greatest difference in power law exponents (over the range of temperatures tested) between the two layers is used, as heat will more easily flow in one direction through the sample.[4] This power law analysis would further help quantify the impact of nonlinearity in temperature-dependent thermal conductivity that is the basis for thermal rectification.[2] While an explicit analysis of power law exponents of metalattice thermal conductivity data is not presented here, the trends of the thermal conductivity data (i.e., their rate of change between 200 and 400 K) for 2 and 30 nm pore sizes, as shown in Fig. 5, suggest that they would make a good match to produce significant thermal rectification for materials tested herein. For both cBN and diamond, the 2 nm metalattices have more negative power law exponents than other materials within the temperature window of interest (175–375 K), while their respective 30 nm metalattices demonstrate more positive power law exponents, which further support their superior performance over other tested materials.

There are still many open questions in terms of how to optimize thermal rectifiers to realize functional phononic devices. Some of these avenues include exploring more complicated system geometries, controlling properties at various length-scales within a system, and further materials research. More specifically, there are many open questions regarding optimizing metalattice-based thermal rectifiers. These questions include performing an in-depth power law analysis to predict heterojunctions with superior performance, exploring optimization and thermal matching of multi-layer systems of three or more layers of different pore sizes (including

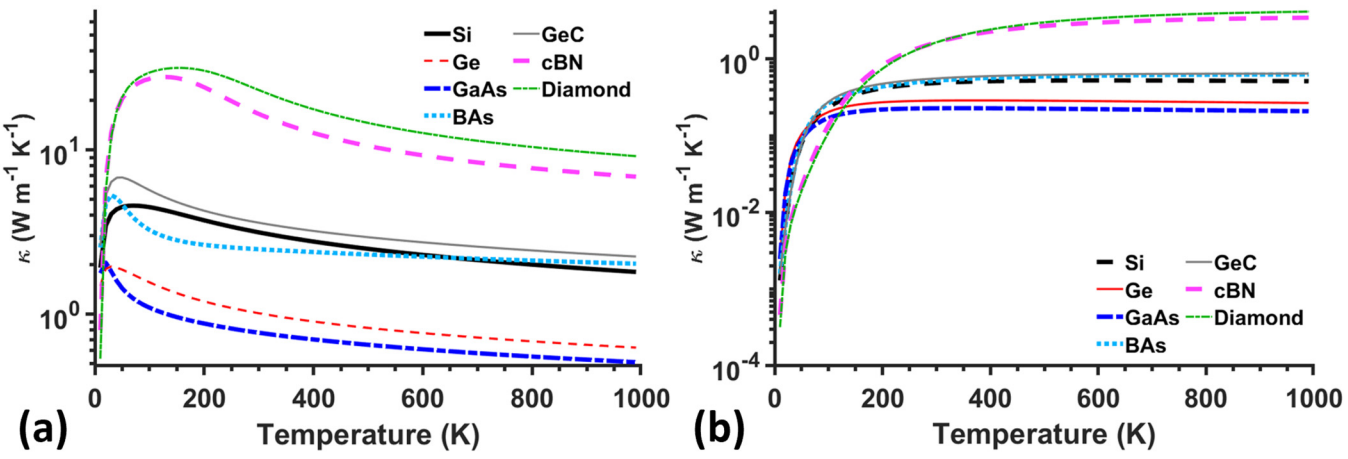

FIG. 5. Temperature-dependent thermal conductivity for metalattices of (a) 2 and (b) 30 nm pore sizes for each tested material.

pore size selection and pore size layer ordering), multi-material systems (including considerations of how phononic mismatch in these systems would affect rectification), and using filled-pore metalattices. A more novel approach may include introducing "rattlers" (e.g., magnetically susceptible particles) in the pores to act as anharmonizers to further increase the nonlinearity and engineered control in the thermal conductivity of metalattices. Finally, for each of these different metalattice cases, further efforts should be made to understand how changing the central temperature, thermal bias, or system geometry may affect thermal rectification.

Future work should pursue experimentally verifying the thermal rectification performance of proposed metalattice structures. According to the data reported in the present work, a diamond metalattice should yield maximum thermal rectification for simulated cases; however, it would require a very high heat flux (3.27×10^{10} W m^{-2} for a 10 μm sample). Silicon, while only providing a maximum rectification value of 19.29%, should still produce a measurable degree of thermal rectification while requiring a much smaller heat flux ($\sim 2 \times 10^{9}$ W m^{-2} for a 10 μm sample). Furthermore, silicon metalattices have already been synthesized and thermally characterized via TDTR,[19] providing further basis in using them as a physical test case.

V. CONCLUSIONS

Through numerical simulation, thermal rectification was calculated for metalattice-based samples with a wide range of sample geometries (number and order of layers), compositions (metalattice pore sizes), and thermal biases. It was found that thermal rectification performance of simple metalattice-based structures can be optimized by utilizing thermally matched material layers. Furthermore, we found by using metalattice structures with controlled pore sizes, a simple geometry, single-material system can exhibit a high degree of thermal rectification. In this work, thermal rectification above 55% is predicted for a bilayer structure composed of 2 and 30 nm pore-sized metalattice layers that are thermally matched using cubic boron nitride or diamond as the basis material. Finally, we predicted that a thermally matched bilayer of 2 nm pore size metalattice and bulk silicon can achieve up to 19% rectification, which has the potential to provide a strong physical test case for measuring thermal rectification in metalattice systems. This work supports further experimentation and optimization of governing parameters of thermal rectifiers for use in advanced phononic applications.

SUPPLEMENTARY MATERIAL

See the supplementary material for further information on validation of the numerical method used here and the process and results of the first-principles-based ballistic modeling performed to generate metalattice material property data.

ACKNOWLEDGMENTS

This research was in-part supported by NSF through The Pennsylvania State University Materials Research Science and Engineering Center through awards DMR-2011839 and DMR-1420620.

AUTHOR DECLARATIONS

Conflict of Interest

The authors have no conflicts to disclose.

Author Contributions

Devon A. Eichfeld: Conceptualization (equal); Formal analysis (lead); Investigation (lead); Methodology (equal); Validation (lead); Writing – original draft (lead); Writing – review & editing (equal). **Weinan Chen:** Data curation (lead); Formal analysis (supporting); Resources (equal); Writing – review & editing (supporting). **Ismaila Dabo:** Data curation (equal); Funding acquisition (lead); Resources (supporting); Validation (supporting). **Brian M. Foley:** Conceptualization (equal); Formal analysis (supporting); Methodology (equal); Supervision (supporting). **Bladimir Ramos-Alvarado:** Formal analysis (supporting); Supervision (lead); Visualization (supporting); Writing – review & editing (lead).

DATA AVAILABILITY

The data that support the findings of this study are available within this article and its supplementary material and from the corresponding author upon reasonable request.

REFERENCES

[1]G. Wehmeyer, T. Yabuki, C. Monachon, J. Wu, and C. Dames, Appl. Phys. Rev. **4**, 041304 (2017).
[2]N. Li, J. Ren, L. Wang, G. Zhang, P. Hänggi, and B. Li, Rev. Mod. Phys. **84**, 1045 (2012).
[3]M. Peyrard, Europhys. Lett. **76**, 49 (2006).
[4]C. Dames, J. Heat Transfer **131**, 061301 (2009).
[5]Z. Cheng, B. M. Foley, T. Bougher, L. Yates, B. A. Cola, and S. Graham, J. Appl. Phys. **123**, 095114 (2018).
[6]R. Dettori, C. Melis, R. Rurali, and L. Colombo, J. Appl. Phys. **119**, 215102 (2016).
[7]W. Zhu, G. Wu, H. Chen, and J. Ren, Front. Energy Res. **6**, 9 (2018).
[8]N. Yang, G. Zhang, and B. Li, Appl. Phys. Lett. **95**, 033107 (2009).
[9]J. Hu, X. Ruan, and Y. P. Chen, Nano Lett. **9**, 2730 (2009).
[10]M. Terraneo, M. Peyrard, and G. Casati, Phys. Rev. Lett. **88**, 094302 (2002).
[11]N. Li and J. Ren, Sci. Rep. **4**, 6228 (2014).
[12]J. Ren and J.-X. Zhu, Phys. Rev. B **87**, 241412 (2013).
[13]J. Ren, Phys. Rev. B **88**, 220406 (2013).
[14]D. Sawaki, W. Kobayashi, Y. Moritomo, and I. Terasaki, Appl. Phys. Lett. **98**, 081915 (2011).
[15]W. Kobayashi, Y. Teraoka, and I. Terasaki, Appl. Phys. Lett. **95**, 171905 (2009).
[16]C. W. Chang, D. Okawa, A. Majumdar, and A. Zettl, Science **314**, 1121 (2006).
[17]H. Wang, S. Hu, K. Takahashi, X. Zhang, H. Takamatsu, and J. Chen, Nat. Commun. **8**, 15843 (2017).
[18]Y. Liu, S. Kempinger, R. He, T. D. Day, P. Moradifar, S.-Y. Yu, J. L. Russell, V. M. Torres, P. Xu, T. E. Mallouk, S. E. Mohney, N. Alem, N. Samarth, and J. V. Badding, Nano Lett. **18**, 546 (2018).
[19]W. Chen, D. Talreja, D. Eichfeld, P. Mahale, N. N. Nova, H. Y. Cheng, J. L. Russell, S.-Y. Yu, N. Poilvert, G. Mahan, S. E. Mohney, V. H. Crespi, T. E. Mallouk, J. V. Badding, B. Foley, V. Gopalan, and I. Dabo, ACS Nano **14**(4), 4235–4243 (2020).
[20]N. A. Roberts and D. G. Walker, Int. J. Therm. Sci. **50**, 648 (2011).

[21]G. Kresse, J. Furthmüller, and J. Hafner, Europhys. Lett. **32**, 729 (1995).
[22]B. M. Foley, H. J. Brown-Shaklee, J. C. Duda, R. Cheaito, B. J. Gibbons, D. Medlin, J. F. Ihlefeld, and P. E. Hopkins, Appl. Phys. Lett. **101**, 231908 (2012).
[23]C. Kittel, *Introduction to Solid State Physics*, 7th ed. (John Wiley and Sons, Inc., 1996).
[24]M. Ustundag, M. Aslan, and B. G. Yalcin, Comput. Mater. Sci. **81**, 471 (2014).
[25]Y. P. Varshni, Physica **34**, 149 (1967).
[26]W. Sekkal and A. Zaoui, New J. Phys. **4**, 9 (2002).